POST-DEADLINE PAPER

(for Session 4)

CURRENT SCINTILLATING FIBRE DETECTORS

L. Linssen
CERN, Geneva, Switzerland

1. PROPERTIES OF SCINTILLATING FIBRES

During the past few years the use of scintillating fibres for the detection of high energy particles has increased considerably thanks to the important progress made in the development of scintillating plastic fibres and optoelectronic technology. The funtioning principle of optical fibres [1] is illustrated in Fig. 1. A fibre consists of a core with refractive index n_1 surrounded by a thin (typically a few wavelengths) optical cladding of refractive index n_2, where $n_2 < n_1$. When a charged particle traverses the core, light is produced in all directions. Only the light inside the cone defined by the critical angle $\theta_c = \sin{-1}(n_2/n_1)$ is trapped inside the fibre. The trapping efficiency in a single direction for circular fibres is therefore $\varepsilon = 0.5(1-n_2/n_1)$. For the fibres commonly used, ε is typically 3%–4%. To prevent crosstalk to neighbouring fibres of the light produced outside the trapping cone the fibre is often surrounded by a thin absorbtive layer called the extra mural absorber (ema).

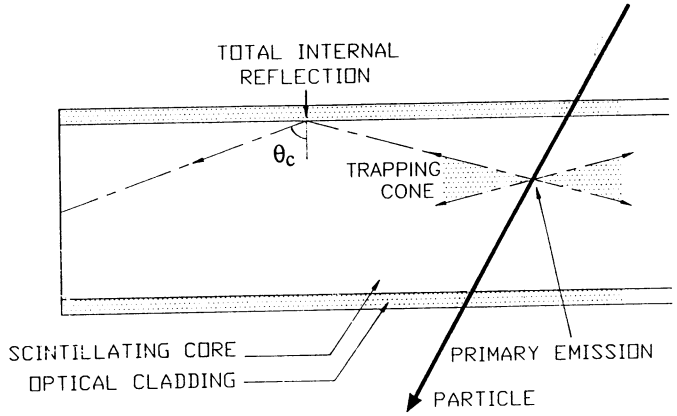

Fig. 1

The core consist of a base material doped with one or more solutes, which shift the emitted light away from the absorption band of the base material. The transfer to the primary solute can be of a dipole–dipole type (Förster mechanism [2]) corresponding to a local reemission of the light. The absorption and reemission by the secondary solute is normally

non–local with a typical mean free path length of ≈ 250 μm. Until recently only glass fibres with a local light emission were known, but the self-absorption due to core impurities was generally high, resulting in attenuation lengths of a few cm only. This has long been a limiting factor to the production of small diameter fibres for high resolution purposes. The application of a primary solute (1–phenyl–3–mesityl–2–pyrazoline, PMP) with a large Stokes shift in plastic fibres has recently given an important improvement in this field [3] (sect. 4). Table 1 gives a summary of the basic properties of a few types of scintillating fibres.

The attenuation of light in optical fibres depends both on the intrinsic absorption properties of the core and on the quality of the core-cladding interface. The self-absorption by the core is caused by the overlap of the emission spectrum of the final solute and the absorption spectrum of the base material. It is therefore wavelength dependent. Short wavelengths are mainly affected. The reflection losses at the core-cladding interface depend on the total number of reflections and therefore on the fibre diameter and on the emission angle. Large emission angles are lost faster. For a reflection coefficient of 0.99995, the corresponding attenuation length for 30 μm diameter fibres is typically 20 cm, for 1 mm diameter fibres it is 6 m. The combination of the above effects results in a light absorption which is fast close to the emission point and slower after the light has traveled some distance along the fibre. As the light produced in the fibre is generally read out from one side only, the opposite fibre–end can be covered by a reflective coating to recuperate part of the light trapped in the other direction, thereby improving the effective attenuation length.

Table 1: Properties of a few types of scintillating fibre

	Glass	Plastic	Plastic
Core material	GS1 + Ce^{3+}	Polystyrene	PS + PBD
		+ PMP	+ POPOP
Cladding material	N15A	PMMA	Polyvinyl acetate
n_1	159	159	159
n_2	151	146	146
Critical angle θ_C (degrees)	72°	67°	67°
Trapping efficiency ε	2.5%	4%	4%
Signal decay	71 ns – 349 μs	3 ns	3 ns
Typical λ_{att}	2 cm	30 cm	1.5 – 2.0 m
For fibre diameter	25μm	30 μm	1 mm

2. DETECTOR APPLICATIONS

In current scintillating fibre detectors various methods of light detection are used:

- photomultipliers, position sensitive photomultpliers,
- photodiodes,
- optical image intensifiers coupled to charged coupled devices or other solid state devices,
- solid state photomultipliers [4].

Detector applications in high energy physics can be found in the field of particle tracking, calorimetry and particle identification. For the particle trackers one can distiguish tracking devices with a typical resolution of a few tenths of a mm and microvertex detectors or active targets with a ten times better resolution. Table 2 gives a (naturally incomplete) list of existing detectors or research groups for the various types of detector applications.

The remainder of this report will be devoted to a more detailed description of the UA2 scintillating fibre detector and of the WA84 active target. For a report on fibre calorimetry I refer to the contribution of H.P. Paar to the proceedings of this conference.

Table 2: Scintillating fibre detectors

TRACKING DETECTORS	
UA2 scintillating fibre detector	[5-8]
Brookhaven AGS 787, k–>πνν̄ target	[9]
SOFIE cosmic ray astrophysics experiment	[10]
MICROVERTEX DETECTORS / ACTIVE TARGETS	
Fermilab E687, photoproduction of charm and beauty	[11]
WA84, beauty search	[12-13]
CERN LAA development work	[14]
FIBRE CALORIMETRY	
Fermilab E774, scifi-ribbon.tungsten calorimeter	[15]
Delphi, small angle tagger	[16]
Jetset Lear, electromagnetic calorimeter	[17]
CERN LAA, electromagn./hadr. calorimeter development	[18]
KEK, electromagn./hadr. calorimeter development	[19]
PARTICLE IDENTIFICATION	
UA2 scintillating fibre detector	[5-8]
Synchrotron radiation electron tagger for SSC	[20]

3. THE UA2 SCINTILLATING FIBRE DETECTOR

3.1 Introduction

The UA2 scintillating fibre detector (SFD) consists of ≈ 60000 plastic fibres of 1 mm diameter and 2.1 m active length. It forms the outer part of the UA2 central detector and provides tracking and particle identification for the detection of 630 GeV antiproton–proton interactions. The SFD has been described in a number of papers [5-8]. For this report we will restrict ourselves to a global desciption of the detector and its performance, occasionally complemented with new results which have not been presented in previous papers.

The fibres are arranged on a cylinder in 24 layers at an average radius of 41 cm around the beam pipe (fig. 2). The 18 innermost layers (6 stereo triplets) are used for tracking. They are surrounded by a 1.5 radiation lengths lead converter. The additional 6 layers (2 stereo triplets) outside the converter are used as a preshower detector to detect the early development of electromagnetic showers. In each stereo triplet one layer of fibres is arranged parallel to the axis of the cylinder. The other two are at angles $\pm\alpha$, where $\alpha = 15.75$ degrees for the tracking part and 21 degrees for the preshower part. The fibres consist of a 1 mm core of polystyrene doped with butyl–PBD and POPOP, surrounded by a 10 μm polyvinyl acetate cladding and an ema of sputtered aluminium (table 1). They are read out from one side. The opposite end is covered by sputtered aluminium (reflectivity 55%) to partly compensate the attenuation of light in the fibres ($\lambda_{att} = 1.65$ m). The light yield at 1.3 m distance from the readout (centre of the detector) for a minimum ionising particle passing through 1 mm fibre thickness is 23 photons of average wavelength 440 nm.

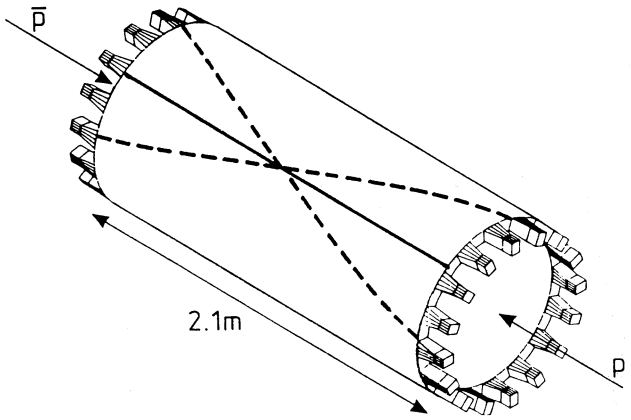

Fig. 2

3.2 The read-out

The signals from the fibres are read out and multiplexed by 32 optoelectronic systems, 16 on each side of the detector. The fibre-ends of ≈ 2000 fibres are grouped in a non–compact rectangular array (50×66 mm^2) by a perforated plate and held at the input of an image intensifier chain. The image intensifiers amplify the light signal by a factor ≈ 40000 and demagnify the area covered by the fibres so that the image fits onto the active area (4.3×5.8 mm^2) of a charged coupled device CCD(*). A single CCD contains 145×208 photosensitive pixels. The light from each individual fibre is spread out over ≈ 12 pixels. Online data compaction is achieved by a purpose built FASTBUS digitiser. The correspondence between the fibres of the detector and the CCD pixels (pixel–to–fibre map) is measured with the aid of 91 fiducial fibres spread uniformly over the face of each image intensifier. These fibres may be illuminated through the aluminium coating at the fibre-end opposite to the read-out.

Each image intensifier system(**) consists of two electrostatically focused image intensifiers (II) and one proximity focused II containing a micro channel plate (MCP), (fig. 3). The image intensifiers are equipped with fast P47 and P46 phosphors with decay times of 50 ns and 100 ns respectively. The basic II properties are summarised in table 3. The second II may be gated off by making its photocathode potential less negative than the MCP entrance voltage.

Earlier studies [5] of the lifetime properties of the MCP showed that the gain loss with integrated current is equally shared between the MCP itself and the photocathode of the second image intensifier. The total gain across II_2 as a function of the integrated current Δq is parametrised as

$$G = G_0 e^{\Delta V/65_e - \Delta q/q_0},$$

where ΔV represents a Voltage change across the MCP in Volts (300 Volts spare for each II_2) and $q_0 = 0.055$ C/cm^2.The large integrated luminosity accumulated over the 1989 run allowed us to monitor the MCP lifetime in $p\bar{p}$ operation. The average gain loss for 29 image intensifiers for which voltages remained unchanged during the accumulation of 3.81 pb^{-1} of $p\bar{p}$ interactions turned out to be as low as 7.8% ±1.3%.

(*) Thomson-CSF 7852.
(**) Delft Electronische Producten,Roden,The Netherlands.

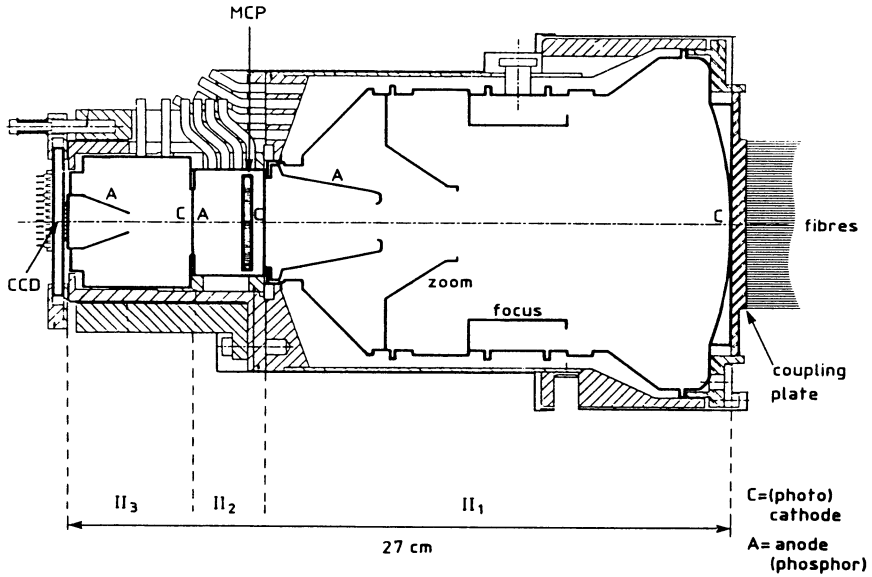

Fig. 3

Table 3: SFD Image Intensifier Parameters

	II_1	II_2	II_3
Input diameter	80 mm	18 mm	18 mm
Output diameter	18 mm	18 mm	7 mm
Photon gain	~ 10	~ 1000	~ 6
Cathode–anode potential	20 kV	7 kV	15 kV
Photocathode	S20	S20	S20
Quantum efficiency	> 13%	16%	16%
Phosphor	P47	P47	P46

The CCD is read out at a speed of 7 MHz, corresponding to a readout time of 5.6 ms for the total image. Antiproton-proton bunch crossings occur every 3.8 μs. If there is no first level trigger after a bunch crossing the CCD image is cleared in 1 μs using the antiblooming drain. If a readout sequence is started after a first level trigger it can be aborted by a second lever trigger veto (after ≈ 1 ms). The CCD signal is received by a FASTBUS digitiser module [8], where it is digitised by an 8–bit flash ADC. The digitiser performs

pedestal subtraction followed by noise compensation using a masked pixel on each CCD line. After a threshold cut of 2 ADC counts the total pulse height for each fibre on the detector is summed using the pixel–to-fibre map. The digitisers reduce the SFD data length per event from ≈ 1 MBytes to ≈ 20 kbytes. The average CCD pedestal noise is $\sigma = 0.35$ ADC counts/pixel. The average signal for a single photoelectron produced at the first II photocathode is 27 counts spread over 12 pixels.

3.3 Detector performance

The intrinsic resolution of the readout is measured using $p\bar{p}$ data. For each hit fibre on the detector 78% of the signal on average is detected in the pixels assigned to that fibre in the pixel–to–fibre map. This corresponds to a point source resolution of 40 μm at the CCD input, to be compared with an average fibre diameter of 75 μm after the II image demagnification.

Figure 4 shows the distribution of the distance between the fitted track and the coordinates measured in the individial layers for the 18–layer tracking part of the SFD. The rms of the fitted Gaussian distribution is 0.39 mm, consistent with a 1 mm fibre diameter. The resolution for a 3–dimensional SFD track segment is about 0.15–mm in Rφ direction and about 0.65 mm in z (along the beam line).

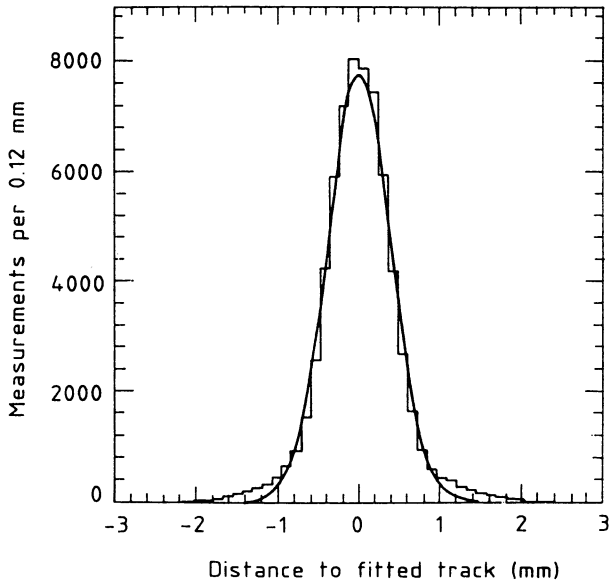

Fig. 4

The average detection efficiency of the SFD is 88% per layer. This includes the average 3% inefficiency per fibre–layer due to the dead space taken by the cladding and occasional fibre to fibre spacing (mainly between the 80–fibre wide ribbons which were used for the detector assembly). The tracking efficiency as measured using cosmic rays is 96%. In $\bar{p}p$ operation the tracking efficiency is 93% due to additional cuts applied in the pattern recognition.

The aim of the preshower detector is to recognize electromagnetic showers from their charge deposition and to measure the starting point of these showers accurately. By requiring a good match between the observed track in the tracking part and the centroid of the electromagnetic cluster in the preshower part one significantly reduces the electron background due to charged hadrons accompanied by a nearby photon. The average charge deposition in the preshower detector for a 40 GeV electron is 20 times higher than for a 40 GeV pion. When a cut is set at 2 MIP the detection efficiency is only 7.3% for a 40 GeV pion, while it is 98.4% for a 40 GeV electron. Figure 5 shows the offset between the SFD track segment and the preshower cluster for 1266 W–>ev decay candidates. Figure 5(a) shows the distribution in Rφ direction, with a fitted rms of 0.4 mm. Figure 5(b) shows the distribution in z, where the resolution is worse due to the 21 degree stereo angle; the rms of the fitted Gaussian is 1.1 mm.

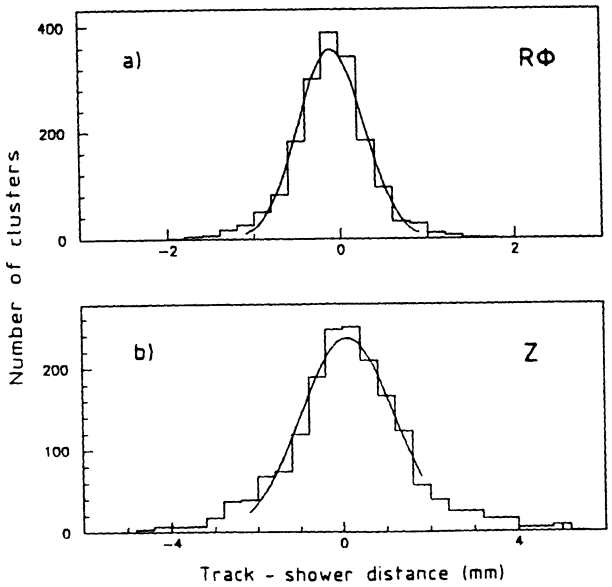

Fig. 5

4. THE WA84 SCINTILLATING FIBRE ACTIVE TARGET

4.1 Introduction

The WA84 experiment at CERN plans to study heavy–flavour physics using a high resolution vertex detector consisting of an active target assembled from coherent bundles of scintillating microfibres [12-13]. The target consists of ≈ 30 μm thin, 5 cm long scintillating fibres running parallel to the incoming beam. Due to the Lorentz boost this target orientation gives a factor ≈ 10 light yield with respect to the orthogonal orientation. The target surface is approximately 5×5 mm^2. The fibre–cores form approximately 70% of the target volume. Different types of scintillating fibres were tried for prototype targets. This section reports mainly on the measurements performed with these prototype targets.

The target test set–up is shown in fig. 6. The target is mounted in a light–tight aluminium box and placed in the beam line. Light emerging from the upstream target end is taken out of the beam by a bend optical taper, which magnifies the optical image by a factor 3.4. The image is then amplified by two proximity focused image intensifiers with a total light gain of ≈ 160. As in the actual WA84 experiment the above elements are exposed to a 1.8 T magnetic field perpendicular to the beam. The light image is then transported by a 2.5 m image guide of 10 μm optical fibres to a second set of image intensifiers outside the magnetic field. It consists of two electrostatic focusing II's to magnify and demagnify the image before and after a factor ≈ 1000 light amplification takes place in a proximity focused II containing an MCP. The MCP is gated on during 1 μs for each first level trigger formed by a set of scintillation counters in the target area. The image is finally recorded by a CCD consisting of 550×288 pixels of dimensions 16×23 μm^2. The CCD is read out at 4 MHz. It contains an antiblooming drain which allows a fast (1 μs) image clear after a second level trigger veto. The light from each optical fibre on the detector is spread over 3.5 pixels on average.

Three different types of target material were compared. The first target is made of Ce^{3+}–doped GS1 glass fibres(*). The individual fibres are square in cross section with a width of 25 μm and they are coated with a very thin opaque layer. The second target is made of plastic fibres of the type SCSN-81T(0.5)(**), which has a 20 times enhanced concentration of the secondary solute, resulting in a mean free path length for the primary light of ≈ 10 μm. After the multibundle production these initially round fibres have an almost hexagonal cross section with a diameter of 30 μm. The third target has the same characteristics as the second one but the fibres cores consist of polystyrene doped with PMP. For the plastic targets the coating of individual fibres with an ema has not been possible yet.

(*) Levy Hill Laboratries Ltd., Waltham Cross, United Kingdom.
(**) Kyowa Gas Chemical Industry Co., Tokyo, Japan.

So far, microbundles of 0.5×0.5 mm^2 were coated with an ema before target assembly. The relevant properties of the different targets are summarised in table 4.

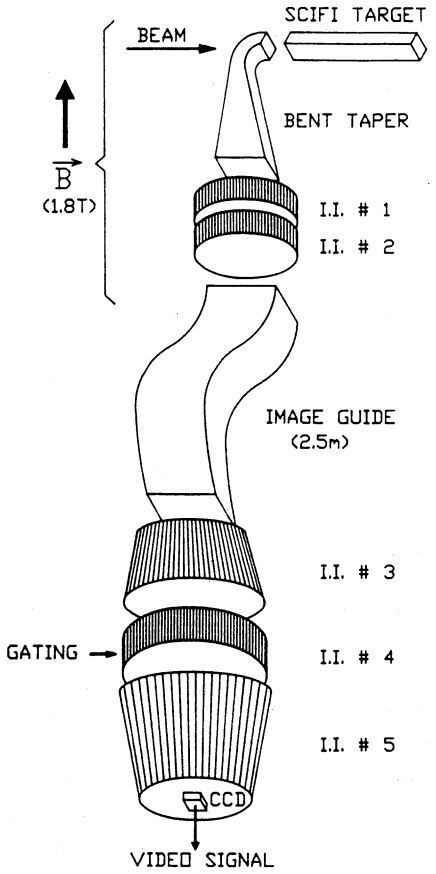

Fig. 6

4.2 Test results

Laboratory studies of the time response of the targets were carried out. The cerium–doped glass fibres showed significant contributions from long–lived components of the light emission. The fast component (decay time 71 ns) accounts for 31% of the total light and the emission continues for more than 1 ms. This leads to superposition of event images and excludes the use of this material for the high rate environment (1.5×10^6 pions/s) of the WA84 experiment. The results are summarised in table 4.

Table 4: Properties of the prototype targets

Fibre core:			
Material	GSI	SCSN – 81T	PMP doped PS
Density (g/m^3)	2.64	1.06	1.06
Shape of cross–section	Square	Hexagonal	Hexagonal
Width (distance between parallel sides) (μm)	25	30	30
Mean refractive index (emission spectrum)	1.59	1.59	1.59
Light decay time (fast component) (ns)	71	2.4	3.0
Percentage of light emitted by fast decay	31%	70%	~ 80%
Wavelength of peak emission (nm)	395	446	425
attenuation length measured in fibres (cm)	2.0	9.4	30.8
Hits density (hits/mm)	0.6	1.4	1.6
Fibre cladding:			
Material	N51A	PMMA	PMMA
Thickness/μm	2	3	3
Mean refractive index (emission spectrum)	1.51	1.46	1.46
Ema present	Yes	No	No

To study the response to single particle tracks the targets were placed at 12° or 20° with respect to the beam line, such that the particle enters and leaves through the target sides, producing straight–line images at the readout face. Tracks are defined by series of clusters of pixel–hits on the CCD. Each of these clusters corresponds to a single photoelectron produced at the photocathode of the first image intensifier. Straight lines are fitted to the pixel hits.

Figure 7 shows the distribution of pulse height traverse to the projected track direction for superimposed tracks. A Gaussian fit to the distribution gives $\sigma = 20$ μm. This result is independent of the fibre-diameter for diameters below 30 μm. To determine the hit density the number of clusters within 3σ around the fitted track are counted for tracks entering the fibres at 25 mm from the readout-face. The resulting hit-densities are given in table 4. Variations in the measured hit–densities are due to differences in the attenuation lengths rather than in the scintillation yields ($\approx$ 2300 photons/mm in the glass, integrating over all the light, and $\approx$ 1800 photons/mm in the plastics). The measured attenuation lengths for the different target vary from 2.0 cm for the glass target to 9.4 cm for SCSN-81T(0.5) and 30.8 cm in the PMP fibres. With a mirrored surface positioned at the non-readout end of the PMP target the hit density is increased to 2.3 mm. Figure 8 shows a few interactions recorded with the target parallel to the beam direction: (a) a 340 GeV pion in the glass target, (b) a 200 GeV hadron in the PMP target with the mirrored surface but with ema at the outer

surface only, (c) a 200 GeV hadron in a PMP target, for which 0.5×0.5 mm^2 microbundles were coated with ema.

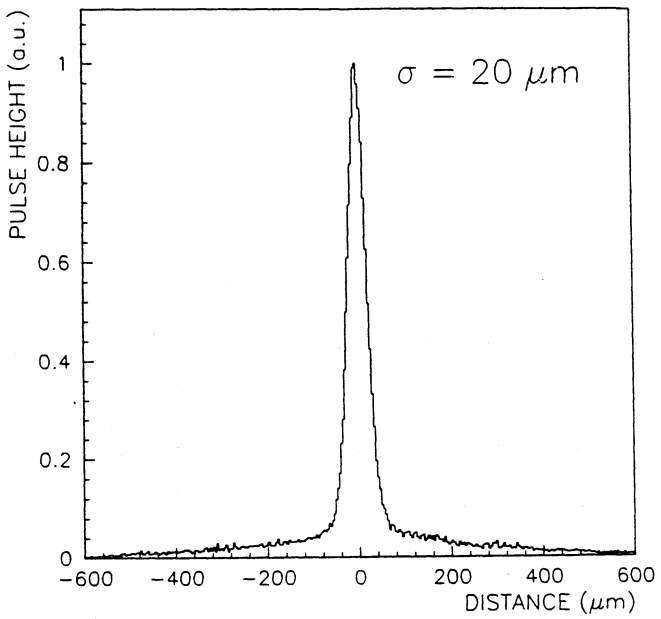

Fig. 7

5. CONCLUSIONS

The application of scintillating fibres in high energy physics experiments is expanding rapidly. We have given a few examples of the use of such detectors in current experiments. Their fast signal development, inherent low occupancy and, thanks to the application of new solutes, radiation hard properties make them very suitable for future use in tracking detectors or calorimeters at SSC/LHC

Acknowledgements

I would like to acknowledge all my colleagues for continuous explanations and discussions, in particular G.Penso for his kind private lecture on the WA84 target.

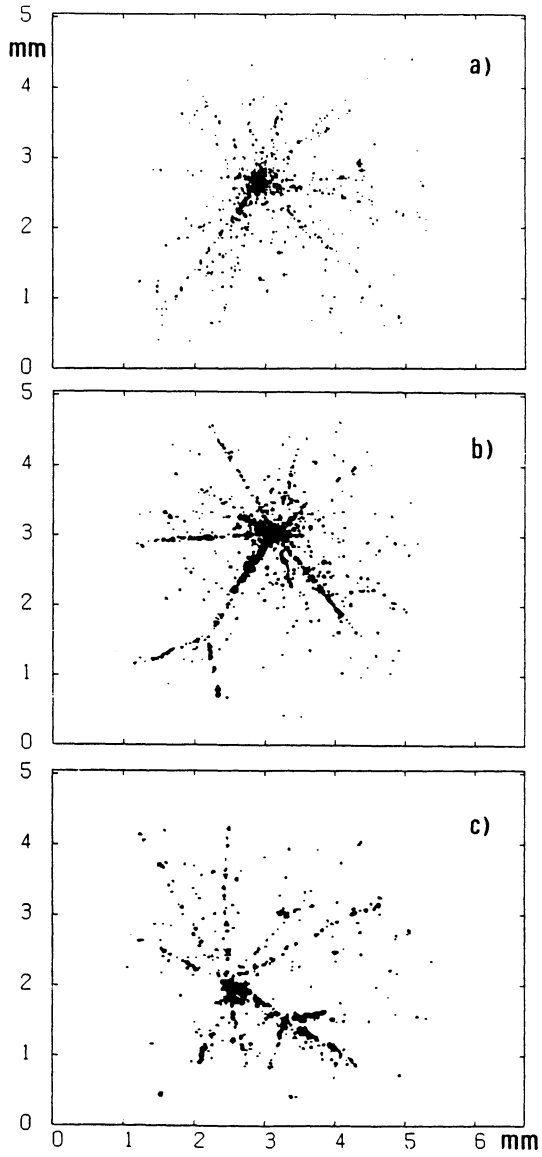

Fig. 8

REFERENCES

[1] Today and tomorrow for scintillating fibre detectors, J.Kirkby, CERN-EP/87-60.

[2] T.Förster, Ann. Physik 2 (1948) 55.

[3] P.Destruel et al., Nucl. Instr. and Meth. A267 (1989) 69.

[4] M.D. Petroff et al., Proc. Workshop on Scintillating Fibre Detector Development for SSC, Fermilab November 1988, 841.

[5] R.Ansorge et al., Nucl. Instr. and Meth. A265 (1988) 33.

[6] J.Alitti et al., Nucl. Instr. and Meth. A273 (1988) 135.

[7] J.Alitti et al., Nucl. Instr. and Meth. A279 (1989) 364.

[8] S.G.Katvers et al., Nucl. Instr. and Meth. A276 (1989) 482.

[9] J.S.Frank et al., Proc. Workshop on Scintillating Fibre Detector Development for SSC, Fermilab November 1988, 359.

[10] A.J.Davis et al., Proc. Workshop on Scintillating Fibre Detector Development for SSC, Fermilab November 1988, 115

[11] R.J.Mountain et al., Proc. Workshop on Scintillating Fibre Detector Development for SSC, Fermilab November 1988, 35.

[12] W.Beusch et al., proposal CERN/SPSC 87-2, SPSC/P 226 (1987)

[13] C.Angelini et al., CERN-EP/89-112.

[14] H.Leutz, contribution to this workshop.

[15] A.Bross, Proc. Workshop on Scintillating Fibre Detector Development for SSC, Fermilab November 1988, 327.

[16] A.Klovning, Proc. Workshop on Scintillating Fibre Detector Development for SSC, Fermilab November 1988, 415.

[17] D.W.Hertzog et al., Proc. Workshop on Scintillating Fibre Detector Development for SSC, Fermilab November 1988, 385.

[18] H.P.Paar, contribution to this workshop.

[19] F.Takasaki, Proc. Workshop on Scintillating Fibre Detector Development for SSC, Fermilab November 1988, 139.

[20] P.Cushman et al., Proc. Workshop on Scintillating Fibre Detector Development for SSC, Fermilab November 1988, 397.